Journal of Physics: Energy

PAPER

OPEN ACCESS

RECEIVED
22 August 2025

REVISED
3 November 2025

ACCEPTED FOR PUBLICATION
9 January 2026

PUBLISHED
21 January 2026

Optimal working conditions for maximal thermoelectric generation via radiative cooling

Jaesuk Hwang[1,*] **and Dario Narducci**[2]

[1] Centre for Quantum Technologies, National University of Singapore, 3 Science Drive 2, Singapore 117543, Singapore
[2] Department of Materials Science, University of Milano Bicocca, v. R. Cozzi 55, I-20125 Milano, Italy
[*] Author to whom any correspondence should be addressed.

E-mail: jhwang@nus.edu.sg and dario.narducci@unimib.it

Keywords: radiative cooling, thermoelectric generation, renewable energy

Supplementary material for this article is available online

Abstract

Thermoelectric generation via radiative cooling holds promise as a renewable electricity source. However, the governing mechanisms have not been fully explained, and the optimal operating conditions are yet to be identified. To address this issue, detailed parametric analyses of the most basic, passive configuration are presented here, where the cold side of the thermoelectric generator is coupled to a radiative cooling surface and the hot side collects heat from the ambient surroundings. We note that the operation deviates significantly from the constant temperature conditions because the radiative cooling power under realistic conditions is not large enough to act as a cold reservoir. The system is thus considered as imperfectly coupled to the reservoirs with a finite thermal conductance. In this regime, the contributions of both electrical and thermal conduction within the thermoelectric generator, along with their interdependence, must be carefully treated to describe the steady-state behaviour. An analytical solution is derived, as an explicit function of system parameters such as the radiative cooling surface area, the degree of thermal insulation of the radiative cooling surface, and the heat transfer coefficient at the hot side. As a result, electrical and thermal impedance matching conditions are presented for the generation of maximum electrical power in terms of these parameters. Our findings serve as a design guide for renewable thermoelectric generation based on the temperature difference between the ambient and the coldness of the sky.

1. Introduction

Renewable energy can be harvested from the naturally occurring radiative heat flows. For example, solar energy, a heat flow from the sun at 6000 K to the earth at approximately 300 K, has served as the staple source of energy via various modes of harvesting, such as photovoltaics generation [1–4], solar thermal generation [5, 6] and solar thermoelectric generation [7–10]. Another major heat flow from the earth at around 300 K to the outer space at 3 K, termed radiative cooling, can also serve as a source of renewable energy, providing a cooling power of tens of Wm^{-2} at the terrestrial level [11, 12].

Recently, there has been growing interest in electricity generation via radiative cooling using a thermoelectric generator (hereafter referred to as a TEG). When the cold side of the TEG is coupled to a radiative cooling substrate facing the sky and the hot side to the ambient air, a temperature gradient develops across the TEG to generate electricity [13–19]. At night, a power density as large as a few hundred $m\mathrm{Wm}^{-2}$ has been demonstrated [20], and it is predicted that the power density could reach the Wm^{-2} level [21], comparable to that of wind power or geothermal energy [22]. Considering the relatively small cost per unit energy, simplicity and scalability, nighttime thermoelectric generation via radiative cooling holds promise as a renewable electricity source complimentary to solar photovoltaics at nighttime [17, 23–28], reducing the need for energy storage devices.

The system considered in this study is depicted in figure 1. The cold side of the TEG is in thermal contact with a radiative cooing surface facing the sky to dissipate heat radiatively into the sky. The hot

surface of the thermoelectric generator, at temperature T_h, is in thermal contact with the ambient at temperature T_{amb}, via a heat sink. By being exposed to the sky, the radiative cooling surface is cooled below the ambient temperature such that, whereas the hot surface temperature is closer to the ambient temperature such that $T_h \approx T_{amb}$. Electricity is generated by the corresponding temperature difference between the hot surface and the cold surface, $\Delta T = T_h - T_c$. It should be noted that if heat were applied to the hot side of the TEG, the generated electricity would be greater than that produced by this configuration. For example, there have been various attempts to combine solar heating and radiative cooling [19, 29–35]. However, no other heat sources or cold sources are considered in this study, in order to rigorously benchmark the renewable energy harvesting potential of the most basic and passive configuration.

This study is motivated by the observation that, to fully characterise the behaviour of the system depicted in figure 1, the dimensionless thermoelectric figure-of-merit $Z\bar{T}$ of the TEG unit and the radiative cooling performance of the radiative cooling surface are, when considered separately, insufficient. Importantly, the operating conditions of the TEG of the system depicted in figure 1 deviate significantly from the constant temperature condition, where large reservoirs of cold and hot sources at fixed temperatures are assumed to be perfectly coupled to each side of the TEG. This is because the radiative cooling power, under realistic conditions, is not large enough to act as a reservoir maintaining a constant temperature at the cold side of the TEG, independently of the internal current and heat conduction from the hot side. To address this issue, the TEG unit is treated as imperfectly coupled to the reservoirs, the cold sky and the ambient, with finite thermal conductance. Derivations are made based on thermal input and output power, without assuming any fixed temperatures on each side of the TEG. In this regime, the thermal conductance across the TEG is an important factor to consider, depending not only on the inherent properties of the TEG but also on the external parameters, such as the load resistance and current. Therefore, to fully explain the steady-state behaviour, the interplay between Fourier's law and Ohm's law must be carefully considered [36]. As a result, the temperature gradient across the TEG ΔT and the electrical and thermal impedance matching conditions are obtained as explicit analytical functions of relevant system and environmental parameters.

Unlike electrical impedance matching, which can be satisfied by adjusting the load resistance, thermal impedance matching conditions must be met at the design stage. Therefore, it is important to understand how the electrical and thermal impedance matching conditions depend on system parameters. To date, the optimal operating conditions have been identified mostly through the numerical solutions of Ioffe's formula [18, 37–39]. Numerical solutions have revealed that the electrical impedance matching conditions obtained depend on the area of the radiative cooling surface, which suggests an interdependence of the electrical and thermal impedance matching conditions. However, the optimal operating conditions in these studies can only be estimated from trends obtained through the repeated trials varying the input values of the system parameters. Furthermore, the intricate relationship between parameters is often hidden in the numerical solutions. To address these issues, this study aims to obtain a fully analytical model of the system to identify optimal working conditions as explicit functions of system parameters such as the area of the radiative cooling surface, the degree of thermal isolation of the radiative cooling surface and the heat transfer coefficient of the heat sink attached to the hot side. The analytical solutions will not only provide insights into the governing mechanisms but also serve as a powerful tool for the ab initio design.

It should be noted that approximate analytical solutions have been obtained from energy balance at the cold surface [21], which explain the measurement results [15, 20]. Whilst providing immediate insights, these analyses do not predict electrical impedance matching conditions and provide approximate estimates of thermal impedance matching conditions. This is because the thermal conductance across the TEG is assumed to be a constant value and that the thermal conductance from the hot side to the ambient air is infinite, thereby largely disregarding the interplay between Fourier's law and Ohm's law, as will be explained in more detail later. The general behaviour of a small-scale test system may be explained with such approximate solutions. However, when scaled up for large-area deployment, analytical functions governing the inter-dynamics of relevant experimental parameters will prove crucial for performance optimisation.

2. Thermoelectric generation via radiative cooling

2.1. Electrical and thermal model

The following analysis evaluates TEG dynamics, where heat is exchanged with two thermostats through contact resistances. Both hot and cold sides exchange heat with the ambient surroundings through the

contact resistances, with the cold side additionally dissipating heat radiatively towards the sky, as depicted in figure 1. Note that the footprints of both cold and hot sides differ from that of the TEG. Thus, a radiative cooling surface, acting effectively as a heat spreader, is assumed to facilitate dissipation (conductive, convective and radiative), whilst a heat sink thermalised to the ambient, acting effectively as a heat concentrator, collects the input thermal power from the ambient (conductive and convective). The electrical and thermal configurations of the system are depicted in figure 2. The heat flux through a TEG unit $\dot{Q}_{\mathrm{TEG}}$ is expressed as [36]:

$$\dot{Q}_{\mathrm{TEG}} = \alpha \bar{T} I + K_{I=0} \Delta T \tag{1}$$

where α is the Seebeck coefficient, $\bar{T}$ is the average temperature $\bar{T} = \frac{T_{\mathrm{h}}+T_{\mathrm{c}}}{2}$, and $K_{I=0}$ is the thermal conductance at zero electrical current (open circuit). The electrical current through the TEG unit I is then given by $I = \frac{\alpha \Delta T}{R+R_{\mathrm{load}}}$, where R is the internal electrical resistance of the TEG unit and R_{load} is the load resistance, and $\Delta T = T_{\mathrm{h}} - T_{\mathrm{c}}$ is the temperature difference across the TEG unit. Then, the thermal conductance across a TEG unit K_{TEG}, defined via $\dot{Q}_{\mathrm{TEG}} = K_{\mathrm{TEG}} \Delta T$, can be written as

$$K_{\mathrm{TEG}} = K_{I=0} \left(1 + \frac{IR}{\alpha \Delta T} Z \bar{T} \right) \tag{2}$$

where the dimensionless thermoelectric figure-of-merit $Z\bar{T}$ is defined with $Z = \frac{\alpha^2}{R K_{I=0}}$. Equation (2) shows that the thermal conductance of the TEG unit K_{TEG} depends not only on inherent properties such as the electrical resistance R and the thermal conductance at zero current $K_{I=0}$, but also on the external parameters such as the load resistance R_{load} and the average temperature $\bar{T}$. Importantly, equation (2) explicitly shows that the thermal conductance across the TEG, K_{TEG}, depends on the current I and the temperature difference ΔT. This elucidates the interplay between the thermal and electrical behaviours, governed respectively by Fourier's law and Ohm's law (see section 1.1 of *supplementary information* for the full derivation of equation (2)). The thermal conductance across the TEG, as described by equation (2), is one of the key differences compared to the solutions in [15, 20, 21], where the thermal conductance is assumed to be a constant value. The difference between the thermal conductance K_{TEG} and the thermal conductance at zero current $K_{I=0}$ can be non-negligible under realistic operating conditions. For example, for a commercially available TEG (Marlow TG12-4), which will be considered as an exemplar system in section 3, the thermal conductance across the TEG unit K_{TEG} can be more than 30% higher than the inherent thermal conductance at zero current, $K_{I=0}$, under impedance matching conditions for optimal electrical power.

The outgoing heat flux at the cold surface of the TEG unit, $\dot{Q}_{\mathrm{out}}$ is given by

$$\dot{Q}_{\mathrm{out}} \approx \dot{Q}_{\mathrm{rad}}(T_{\mathrm{amb}}) - (K_{\mathrm{rad}} + K_{\mathrm{c}}) \left(\frac{K_{\mathrm{TEG}} + K_{\mathrm{h}}}{K_{\mathrm{h}}} \right) \Delta T \tag{3}$$

where the first term $\dot{Q}_{\mathrm{rad}}(T_{\mathrm{amb}})$ represents the net radiative cooling power of the radiative cooling surface. It is defined as the difference between the total flux emitted by the radiative cooling surface at ambient temperature T_{amb} and the total flux of atmospheric emission absorbed by the radiative cooling surface. The net radiative cooling power $\dot{Q}_{\mathrm{rad}}(T_{\mathrm{amb}})$ is therefore a quantity characterising the radiative cooling part of the system. It is determined both by the material property of the radiative cooling surface and by the local sky conditions, and it is independent of the properties of the TEG.

The thermal emission from the radiative cooling surface can be assessed by integrating the thermal emission of the radiative cooling surface $\sigma \varepsilon_{\mathrm{rcs}}(\lambda, \theta) T_{\mathrm{c}}^4$ over wavelength λ and angle θ, where σ is the Stefan-Boltzmann constant and $\varepsilon_{\mathrm{rcs}}(\lambda, \theta)$ is the emissivity of the radiative cooling surface. The atmosphere appears semi-transparent about the zenith direction within the wavelength range from 8 to 14 μm, the so-called 'sky window,' whereas the atmosphere outside the sky window appears as opaque as a blackbody at ambient temperature T_{amb}. The atmospheric emission can be modelled as a function of ambient temperature and the sky emissivity [40, 41], simulated [42] or directly measured [43]. In general, the atmospheric emission depends heavily on the local conditions such as humidity or cloud coverage [44–46]. The detailed methods for evaluating the net radiative cooling power $\dot{Q}_{\mathrm{rad}}(T_{\mathrm{amb}})$ have been given in numerous other references, for example, [12, 47], and will not be repeated here (see sections 1.2 and 1.3 of supplementary information for further details). It is only mentioned here that the sky appears colder than the ambient air and the total absorbed atmospheric emission at each measurement location, affected by the weather condition and the cloud coverage, is reflected in the

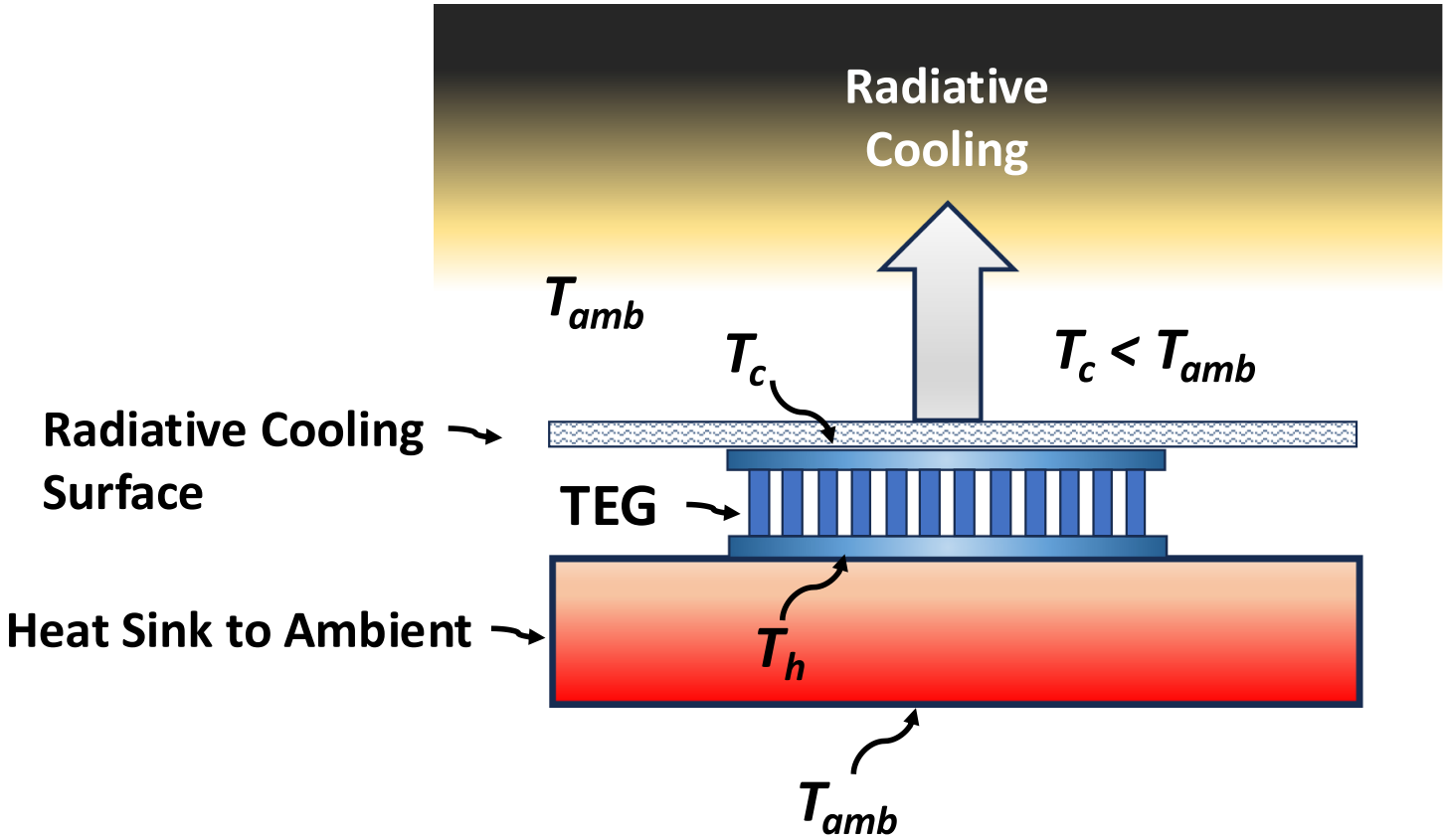

Figure 1. Sketch of the system considered in this study. A radiative cooling surface is attached to the cold surface of a TEG and disposed to face the sky. The cold surface of the TEG is in thermal contact with a radiative cooing surface which dissipates heat radiatively into the sky. See text for details.

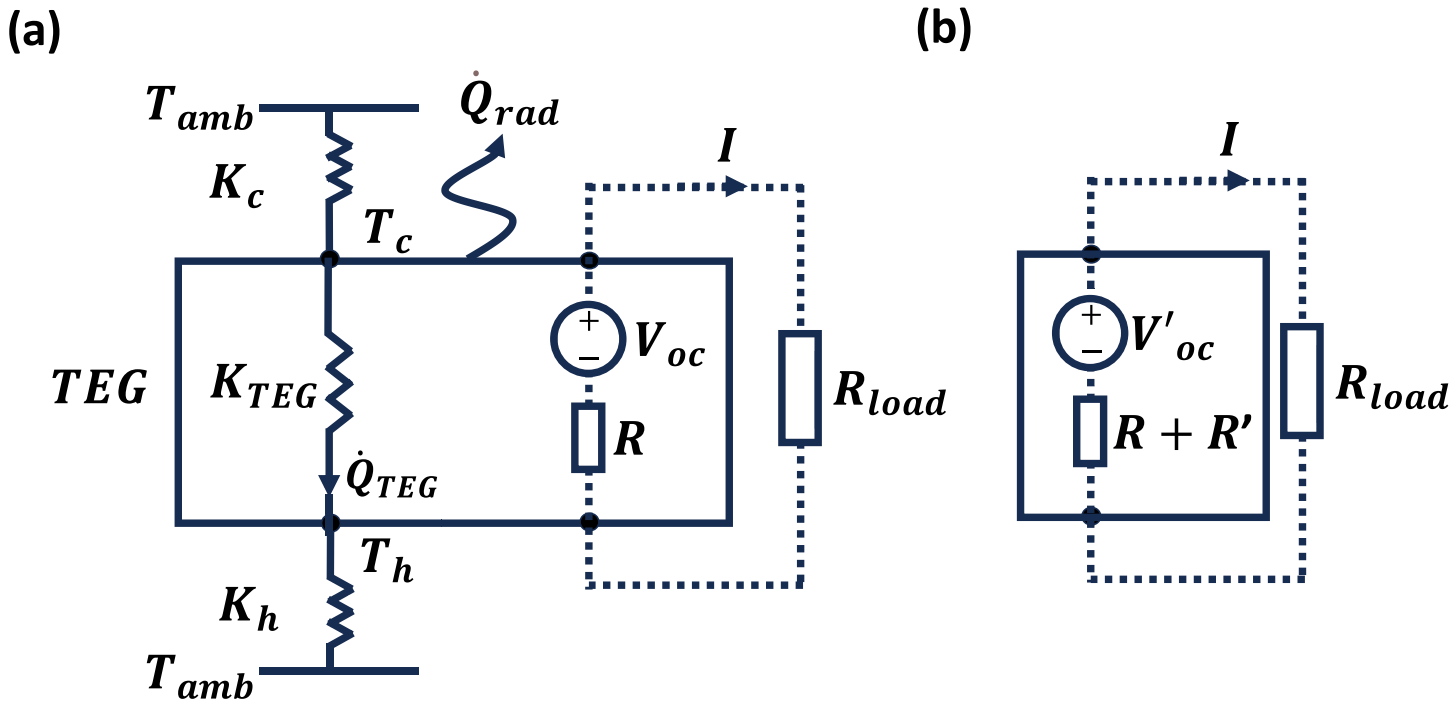

Figure 2. (a) Schematics of the electric and thermal configurations of the system. (b) Thevenin-equivalent circuit of the electrical configuration shown in (a).

net radiative cooling power $\dot{Q}_{\mathrm{rad}}(T_{\mathrm{amb}})$. In the temperature range under discussion, the thermal emission spectrum given by the emissivity $\varepsilon_{\mathrm{rcs}}(\lambda,\theta)$ is nearly disjoint with the solar spectrum. Therefore, $\varepsilon_{\mathrm{rcs}}(\lambda,\theta)$ fully characterises the thermal emission from the radiative cooling surface but does not define its response to the solar irradiation. For example, a radiative cooling surface with a given emissivity spectrum $\varepsilon_{\mathrm{rcs}}(\lambda,\theta)$ can be fully reflective or fully absorptive of the solar irradiation, therefore can have any colour in the visible spectrum. The term 'blackbody' in this study thereby refers to a surface with unity emissivity where, not a black surface in appearance. The heat gain on the radiative cooling surface due to the absorption of solar irradiation is characterised by P_{solar}, independent of the small temperature change ΔT. The solar heat gain is included to reduce the net radiative cooling power $\dot{Q}_{\mathrm{rad}}(T_{\mathrm{amb}})' = \dot{Q}_{\mathrm{rad}}(T_{\mathrm{amb}}) - P_{\mathrm{solar}}$.

With regard to the second term of equation (3), the heat dissipation at the cold surface occurs via two channels, radiative and non-radiative (via conduction, convection or both), with radiative thermal conductance K_{rad} and with effective thermal conductance K_{c}, respectively. Both the radiative thermal conductance K_{rad} and the effective thermal conductance K_{c} are proportional to the area of the radiative cooling surface. The radiative contribution is approximated as linearly dependent on the temperature, with radiative thermal conductance K_{rad} related to the average emissivity value $\varepsilon_{\mathrm{rcs}}$, via $K_{\mathrm{rad}} = 4\varepsilon_{\mathrm{rcs}}\sigma T_{\mathrm{amb}}^3 A$. It should be noted that this approximation does not assume a uniform emissivity spectrum. As discussed previously, the wavelength- and angle-dependence of the emissivity $\varepsilon_{\mathrm{rcs}}(\lambda,\theta)$ must be integrated in order to determine the average emissivity $\varepsilon_{\mathrm{rcs}}$ and the net radiative cooling power $\dot{Q}_{\mathrm{rad}}(T_{\mathrm{amb}})$. The linear approximation assumes only that the radiative cooling power varies linearly from $\dot{Q}_{\mathrm{rad}}(T_{\mathrm{amb}})$ with small ΔT, with the average emissivity $\varepsilon_{\mathrm{rcs}}$ being the key parameter in the proportionality coefficient. Under this approximation, the average emissivity $\varepsilon_{\mathrm{rcs}}$ and the net radiative cooling power $\dot{Q}_{\mathrm{rad}}(T_{\mathrm{amb}})$ define the radiative cooling part of the system. This approximation will be justified further in equation (7). The effective heat conductance K_{c} at the cold surface is determined by the degree of thermal insulation of the radiative cooling surface from the environment. It should be noted that the outgoing heat flux at the cold surface of the TEG according to equation (3) also depends on the thermal conductance K_{h} at the hot surface of the TEG and the thermal conductance across the TEG K_{TEG}. The hot surface of the TEG unit receives heat from the ambient, for example via a finned heat sink for natural convection. The thermal conductance is defined by the capacity of the heat sink attached to the hot side of the TEG. In general, the thermal conductance K_{h} should be maximised such that the hot surface temperature T_{h} is as nearly equal to as possible to the ambient temperature T_{amb}. However, the minute difference is crucial for the accurate assessment of system dynamics. Both thermal conductances K_{c} and K_{h} represent the linear dependence of the heat transfer to and from the environment upon the temperature difference, according to Fourier's law of heat conduction. Equation (3) rests upon two reasonable approximations: firstly, it is assumed that the temperature drop from ambient temperature to the radiative cooling surface temperature is much smaller than the ambient temperature, namely, $T_{\mathrm{amb}} - T_{\mathrm{c}} \ll T_{\mathrm{amb}}$; secondly, as in Apertet *et al* [36] it is stipulated that the output electrical power $P = \dot{Q}_{\mathrm{in}} - \dot{Q}_{\mathrm{out}}$ is negligible compared with $\dot{Q}_{\mathrm{out}}$, such that $K_{\mathrm{TEG}}\Delta T \approx \dot{Q}_{\mathrm{out}}$. The second approximation is valid for most realistic thermoelectric generators, especially when the temperature difference ΔT is much smaller than T_{amb}, whereby the Carnot efficiency and the Novikov–Curzon–Ahlborn efficiency are small, and the actual efficiency is even smaller (see sections 1.2 and 1.3 of supplementary information for the derivation of equation (3)).

The temperature difference across the TEG unit ΔT can be obtained from $\dot{Q}_{\mathrm{out}} \approx K_{\mathrm{TEG}}\Delta T$ using equations (2) and (3). The corresponding open circuit voltage $V_{\mathrm{oc}} = \alpha\Delta T$ is then:

$$V_{\mathrm{oc}} = \alpha\frac{K_{\mathrm{h}}\dot{Q}_{\mathrm{rad}}(T_{\mathrm{amb}})}{K_{I=0}(K_{\mathrm{crad}}+K_{\mathrm{h}})+K_{\mathrm{crad}}K_{\mathrm{h}}} - IR\frac{K_{I=0}(K_{\mathrm{crad}}+K_{\mathrm{h}})}{K_{I=0}(K_{\mathrm{crad}}+K_{\mathrm{h}})+K_{\mathrm{crad}}K_{\mathrm{h}}}Z\bar{T} \tag{4}$$

where $K_{\mathrm{crad}} = K_{\mathrm{rad}} + K_{\mathrm{c}}$. Equation (4) is in the form of $V_{\mathrm{oc}} = V'_{\mathrm{oc}} - IR'$ with

$$V'_{\mathrm{oc}} = \frac{\alpha\dot{Q}_{\mathrm{rad}}(T_{\mathrm{amb}})}{K_{\mathrm{crad}}}\frac{K_{\mathrm{contact}}}{K_{I=0}+K_{\mathrm{contact}}} \tag{5}$$

$$R' = R\frac{K_{I=0}}{K_{I=0}+K_{\mathrm{contact}}}Z\bar{T} \tag{6}$$

where $K_{\mathrm{contact}} = \frac{K_{\mathrm{crad}}K_{\mathrm{h}}}{K_{\mathrm{crad}}+K_{\mathrm{h}}}$, defined here as the 'contact thermal conductance,' is the combined thermal conductance to the reservoirs at both surfaces of the TEG, which includes the radiative, conductive, and convective channels at the hot and cold surface of the TEG. K_{crad} represents the serial combination of

the radiative and conductive/convective channels at the cold surface. K_{contact} represents the parallel combination of K_{h} and K_{crad}. The contact thermal conductance K_{contact} represents the overall thermal conductance, reflecting the finite degrees of heat transfer to and from the two reservoirs considered here, the cold sky and the ambient environment. The relative magnitude of K_{contact} to $K_{I=0}$ is one of the key parameters in determining the thermal impedance matching. It should be noted that the contact thermal conductance K_{contact} is not limited by the interfacial thermal resistances between the surfaces of the TEG and the heat sink. For the purpose of this discussion, these interfacial thermal resistances are not included in the contact thermal conductance K_{contact} as they can be rendered negligible compared with K_{contact} through proper application of heat sink compound [15, 20]. Equations (4)–(6) show that the voltage source provided by the TEG unit can no longer be considered perfect, given its dependence upon the current I. Instead, the electrical configuration of the TEG unit can be represented as the Thevenin equivalent circuit, comprising a perfect voltage source with an open-circuit voltage V'_{oc} and a resistance $R+R'$ connected in series (figure 2(b)). This is a direct consequence of imperfect thermal coupling of the TEG unit to the reservoirs [36] and is considered the physical origin of the non-trivial electrical and thermal impedance matching conditions, which are discussed in the following section.

The temperature difference ΔT can be restated in a form independent of I from equation (4):

$$\Delta T = \frac{\dot{Q}_{\text{rad}}(T_{\text{amb}})}{K_{\text{crad}}} \frac{(1+m)\frac{K_{\text{contact}}}{K_{I=0}}}{\left((1+m)\left(1+\frac{K_{\text{contact}}}{K_{I=0}}\right)+Z\bar{T}\right)} \tag{7}$$

where the ratio $m = \frac{R_{\text{load}}}{R}$ represents the degree of electrical impedance matching. Equation (7) demonstrates that the temperature difference ΔT depends explicitly upon both the degree of electrical impedance matching m and the degree of thermal impedance matching $\frac{K_{\text{contact}}}{K_{I=0}}$. In the linear limit–i.e. the first approximation used in deriving equation (3)–the ratio $\frac{\dot{Q}_{\text{rad}}(T_{\text{amb}})}{K_{\text{crad}}}$ represents the largest temperature reduction achievable by the radiative cooling surface in isolation, when uncoupled to the TEG. Equation (7) shows that the temperature difference ΔT, when coupled to the TEG, always remains below this value. This is owing to the finite thermal conductance across the TEG unit. The thermal conduction pathway from the ambient through the TEG unit to the radiative cooling surface persists as the principal source of heat gain even in the case of high-vacuum shielding, whereby all other conductive heat gains to the radiative cooling surface are suppressed [19, 20]. It is also noted that ΔT in equation (7) is explicitly dependent on K_{h} via K_{contact}, which is disregarded in the approximation made for ΔT in [15, 20, 21]. Equation (7) also further justifies the first approximation made for equation (3), $\Delta T \ll T_{\text{amb}}$. Even the state-of-the-art radiative cooling surfaces can cool themselves only by several degrees below the ambient temperature in most climates [48, 49]. Equation (7) indicates that ΔT will be smaller still. Furthermore, equation (7) shows that even when a vacuum enclosure is employed, $K_{\text{c}} \to 0$, the amplification of ΔT is modest because of the heat conduction across the TEG unit. Consequently, across all reasonable parameter ranges, ΔT remains substantially smaller than T_{amb}. The validity of the two approximations used in equation (3) will be examined again in sections 3.2 and 3.3.

2.2. Maximisation of electrical power and efficiency

According to equation (6), the effective electrical resistance of the TEG unit R_{TEG} increases by the Thevenin equivalent circuit resistance R' (figure 2(b)) and is given by $R_{\text{TEG}} = R + R'$. The electrical power P at the load, $P = \frac{{V'_{\text{oc}}}^2 R_{\text{load}}}{(R_{\text{TEG}}+R_{\text{load}})^2}$, is then maximised when $R_{\text{load}} = R_{\text{TEG}} = R + R'$. The electrical impedance matching condition for maximum electrical power is thereby given by

$$m = 1 + \frac{Z\bar{T}}{1+\frac{K_{\text{contact}}}{K_{I=0}}}. \tag{8}$$

This result indicates that the optimal load resistance, R_{load}, is greater than the internal electrical resistance of the TEG, R, as is also predicted by the numerical solution of Ioffe's formula [39]. In the limit where the contact thermal conductance, K_{contact}, approaches infinity, or under constant temperature conditions, the electrical impedance matching condition converges to $m = 1$. Approximating the electrical power as proportional to $(\Delta T)^2$ [15, 20, 21] also leads to the electrical impedance matching condition at $m = 1$.

The thermal impedance matching condition is obtained by optimising the electrical power P with respect to $K_{I=0}$ for a fixed K_{contact} and given by

$$\frac{K_{I=0}}{K_{\text{contact}}} = \frac{1+m}{1+m+Z\bar{T}} \tag{9}$$

namely for $K_{\text{contact}} = K_{\text{TEG}}$. The simultaneous thermal and electrical impedance matching conditions, satisfying both equations (8) and (9), are given by

$$\frac{K_{\text{contact}}}{K_{I=0}} = \sqrt{1+Z\bar{T}} \text{ and } m = \sqrt{1+Z\bar{T}}. \tag{10}$$

At the condition satisfying the simultaneous electrical and thermal impedance matching condition according to equation (10), the temperature difference ΔT according to equation (7) becomes $\frac{\dot{Q}_{\text{rad}}(T_{\text{amb}})}{2K_{\text{crad}}}$, half of the largest temperature reduction achievable with the given radiative cooling surface. At the simultaneous electrical and thermal impedance matching condition, the maximum electrical power is given by

$$P_{\max} = \frac{\alpha^2}{4R}\left(\frac{\dot{Q}_{\text{rad}}(T_{\text{amb}})}{K_{\text{crad}}}\right)^2 \frac{\sqrt{1+Z\bar{T}}}{\left(1+\sqrt{1+Z\bar{T}}\right)^2}. \tag{11}$$

The maximum electrical power depends on the internal parameters of the TEG, namely the dimensionless figure-of-merit $Z\bar{T}$, the Seebeck coefficient α and the internal electrical resistance R but *not* on K_{h}, which is proportional to the heat transfer coefficient at the hot surface of the TEG to the ambient. This explains partly why the solutions in [15, 20, 21], which disregard the heat transfer coefficient at the hot surface to the ambient, are still effective in estimating the maximum electrical power. However, as shown in equations (8)–(10), the electrical and impedance matching conditions are also dependent on the heat transfer coefficient of the heat sink at the hot surface. The examples illustrating this dependence will be presented in section 3.2.

So far, the optimisation conditions related to the maximisation of generated electrical power. Instead, the efficiency $\eta = \frac{P}{\dot{Q}_{\text{TEG}}}$ can be maximised at the electrical impedance matching condition given by

$$m = \sqrt{\left(1+Z\bar{T}\right)\left(1+\frac{Z\bar{T}}{1+K_{\text{contact}}/K_{I=0}}\right)}. \tag{12}$$

The simultaneous thermal and impedance matching conditions for the maximum efficiency can be obtained numerically by optimising η in a similar fashion as equations (9) and (10). It is mentioned in passing when the thermal input from the ambient to the hot side of the TEG is not considered as in [15, 20, 21], the maximum efficiency condition of operation cannot be defined.

3. Exemplar system analysis

In what follows we will consider the power generated by a commercially available TEG (Marlow TG12–4, 3 cm × 3 cm, 127 legs) whose specifications ($K_{I=0} = 0.251$ W K^{-1}, $R = 3.377$ Ω, $\alpha = 0.046$ V K^{-1}, $Z\bar{T} = 0.764$ at $\bar{T} = 300$ K) were reported in previous works [39, 50]. The TEG consists of serially-connected 127 thermocouples made of n-doped and p-doped Bismuth Telluride (Bi_2Te_3) alloys. Each of the 127 p–n legs is 1.6 mm tall and disposed over a 3 cm × 3 cm area between two 0.9 mm thick Aluminium Oxide sheets, which act as the cold side and the hot side of the TEG. A near-blackbody radiative cooling surface with the average emissivity = 0.95 will be considered as an example such that the radiative heat transfer coefficient $h_{\text{rad}} = \frac{K_{\text{rad}}}{A} = 4\varepsilon_{\text{rcs}}\sigma T_{\text{amb}}^3$ is 6.00 Wm^{-2}K^{-1} at ambient temperature $T_{\text{amb}} = 303.15$ K (see section 1.3 of supplementary information for additional details). Such radiative cooling surface can be implemented with a black acrylic paint on a thin metallic plate, such as copper plate.

The atmospheric emission of a clear sky can be determined via the atmospheric emissivity as a function of the dew point temperature T_{dew}, given by $\varepsilon_{\text{atm}} = 0.741 + 0.0062\,(T_{\text{dew}} - 273.15)$ [51, 52]. It is understood that the most accurate values of the sky emissivity are obtained through direct measurements. For example, clouds further increase the atmospheric emissivity beyond the clear sky values, thereby reducing the radiative cooling power [44]. Here, two extreme cases of clear sky examples will be considered as representative atmospheric conditions. To model the atmosphere in a dry climate, a relative humidity of 25% is assumed, corresponding to the dew point temperature $T_{\text{dew}} = 281.0$ K at $T_{\text{amb}} = 303.15$ K. In the other extreme, for a humid climate, a relative humidity of 85% is assumed, which corresponds to the dew point temperature $T_{\text{dew}} = 300.3$ K, at the same ambient temperature $T_{\text{amb}} = 303.15$ K. We will refer to these two atmospheric conditions as 'desert' and 'tropics,' respectively. Thus, $\dot{Q}_{\text{rad}}(T_{\text{amb}})$ is 95.69 W for the desert and 41.25 W for the tropics, assuming a radiative cooling surface area A of 1 m^2, with values scaling proportionally to the radiative cooling surface area A.

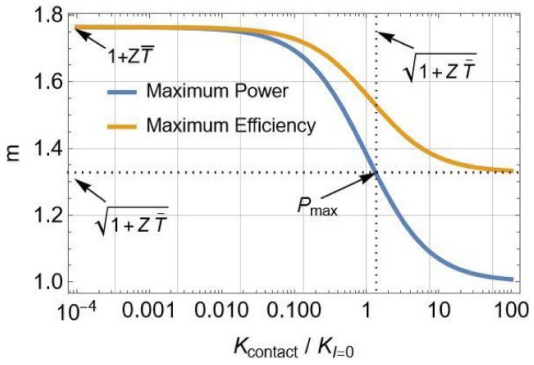

Figure 3. Electrical impedance matching conditions for the maximum electrical power and the maximum efficiency, plotted as a function of the degree of thermal impedance matching $K_{\text{contact}}/K_{I=0}$.

3.1. Maximum power vs maximum efficiency

We first demonstrate that the impedance matching conditions for maximising electrical power and efficiency differ from one another for the exemplar system under consideration. Figure 3 presents plots for two m values, representing the electrical impedance matching condition for maximising power according to equation (8), the blue solid line, and the electrical impedance matching condition for maximising efficiency according to equation (12), the orange solid line, respectively. The two m values are plotted as a function of $K_{\text{contact}}/K_{I=0}$, representing the degree of thermal impedance matching. When the contact conductance K_{contact} is small compared with the TEG conductance $K_{I=0}$, both m values converge to $1+Z\bar{T}$. In other words, when the couplings to the reservoirs are weak, there is no difference between the electrical impedance matching conditions for maximum power and maximum efficiency. In this limit, the so-called constant flux condition, the heat flux through the TEG $\dot{Q}_{\text{TEG}}$ is fixed and the conditions for maximising efficiency $\eta = \frac{P}{\dot{Q}_{\text{TEG}}}$ and electrical power P are manifestly the same [53]. However, when K_{contact} becomes comparable with $K_{I=0}$, the two m values begin to differ from each other. When K_{contact} is much larger than $K_{I=0}$, corresponding to the constant temperature condition, or to the case in which both TEG surfaces are coupled to the thermostats with large thermal conductance, the m value for maximum power converges to 1, whereas the electrical matching ratio for maximum efficiency converges to [54].

The point on the maximum power curve, labelled P_{max}, corresponds to the condition for maximum electrical power, optimised simultaneously in terms of electrical and thermal impedances according to equation (10). It is noticed that at this point of thermal impedance matching, represented by the vertical dotted line, the load resistances R_{load} for the simultaneous impedance matching for maximum efficiency differs from that for maximum electrical power. This suggests that in practical systems, it is difficult to satisfy the operating conditions for maximum power and for maximum efficiency simultaneously. Since input power is attainable at no cost, we will focus mainly on the impedance matching conditions for maximum power rather than efficiency.

The thermal impedance matching conditions must be determined at the design stage because the parameters relating to the thermal impedance matching conditions are difficult to measure and not straightforward to adjust once the device is deployed. In contrast, the electrical impedance matching conditions according to equations (8) and (12) can be found even after deployment by varying the external load resistance R_{load}. Therefore, in what follows, the electrical impedance matching conditions will be considered as satisfied whilst the dependence of the electrical power on the thermal parameters determining K_{contact} will be explored.

3.2. Optimal area of radiative cooling surface

According to equations (9) and (10), the thermal impedance matching conditions depend only on K_{crad} and K_{h}. The former is proportional to the area of the radiative cooling surface A as

$$K_{\text{crad}} = K_{\text{c}} + K_{\text{rad}} = h_{\text{cold}}A + h_{\text{rad}}A \tag{13}$$

where $h_{\text{rad}} = 4\varepsilon_{\text{rcs}}\sigma T_{\text{amb}}^3$ and h_{cold} is the heat transfer coefficient into the radiative cooling surface, determined by the degree of thermal insulation around the radiative cooling surface (see section 1.3 of *supplementary information* for details). For the convenience of calculation, it is assumed that the overall footprint of the device is delimited by the radiative cooling surface area A and that the heat sink

attached to the hot side of the TEG is also bounded within that footprint, as depicted in figure 1. Then the thermal conductance to the hot side of the TEG K_h can be written as

$$K_h = h_{hot} A \tag{14}$$

where the heat transfer coefficient h_{hot} is the heat transfer coefficient of the heat sink to the ambient, reflecting the degree of thermal exchange via conduction and convection to the environment. This stipulation also covers the case where the lateral dimension is smaller than the radiative cooling surface area A, as the heat transfer coefficient h_{hot} can be simply adjusted to correctly represent the conductance K_h. From equations (13) and (14), $K_{contact}$ is a function h_{cold} and h_{hot} and proportional to the radiative cooling surface area A. In the example considered, $\varepsilon_{rcs} = 0.95$ and $h_{rad} = 6.00\ \mathrm{Wm^{-2}K^{-1}}$ at $T_{amb} = 303.15\ K$. Therefore, three experimental parameters control the thermal impedance matching conditions: the radiative cooling surface area A and the heat transfer coefficients h_{cold} and h_{hot}.

From equation (10), the optimal area of the radiative cooling surface A_{opt} can be obtained at each value of h_{cold} and h_{hot}. Figure 4(a) shows the plot of the optimal area A_{opt} as a function of h_{cold} and h_{hot} while figure 4(b) shows the same plot but in terms of the optimal radius r_{opt} given by $A_{opt} = \pi r_{opt}^2$, assuming that the radiative cooling surface is of a circular shape. h_{cold} spans values from 0 to 10 $\mathrm{Wm^{-2}K^{-1}}$ while h_{hot} ranges over values from 10 to 200 $\mathrm{Wm^{-2}K^{-1}}$. When both heat transfer coefficients are set to 10 $\mathrm{Wm^{-2}K^{-1}}$, they represent the case of a system exposed to the surroundings without any thermal insulation. Note that h_{cold} can approach zero as h_{cold} can be made negligible by enclosing the radiative cooling surface within a vacuum chamber with an infrared-transmitting window evacuated to a pressure below 10^{-5} torr [19, 20, 44, 55–57]. In the other extreme, h_{hot} at 200 $\mathrm{Wm^{-2}K^{-1}}$ corresponds to a highly efficient heat transfer from the hot side of the TEG to the environment facilitated, for example, by a large convective heat sink exposed to strong winds with a high thermal mass thermalised with the ambient surroundings.

From figure 4(a), it is observed that the optimal area A_{opt} increases as h_{cold} and h_{hot} decrease. Figure 4(b) shows that the optimal radius r_{opt} ranges from approximately 8 cm to 16 cm- significantly larger than the footprint of the TEG unit, 3 cm by 3 cm, thus confirming the assumption that the footprint is bounded by the area of the radiative cooling surface A but should exceed that of the TEG itself. When the radiative cooling surface is maintained at ambient conditions and the hot surface is exposed to the ambient air via a small, finned heat sink–corresponding to the heat transfer coefficient values around $h_{cold} = h_{hot} = 10\ \mathrm{Wm^{-2}K^{-1}}$ - the optimal radius of the near-blackbody radiative cooling surface ($\varepsilon_{rcs} = 0.95$) is 13.1 cm, regardless of the climate conditions. In the limit where h_{hot} is very large, the optimal area A_{opt} is given by

$$A_{opt,\, h_{hot}\to\infty} = \frac{K_{I=0}\sqrt{1+Z\bar{T}}}{h_{rad} + h_{cold}}. \tag{15}$$

This indicates that the optimal area A_{opt} is proportional to the thermal conductance across the TEG at zero current $K_{I=0}$. This suggests that as both surfaces of the TEG become more thermally decoupled, the overall footprint of the device can be reduced. It is also worth noting that the optimal area A_{opt} must be larger when a vacuum enclosure is used (i.e. $h_{cold} \to 0$) compared to when the radiative cooling surface is exposed to the ambient surroundings. For example, with and $h_{hot} = 10\ \mathrm{Wm^{-2}K^{-1}}$, the optimal radius is 16.8 cm. However, as we will see, the vacuum enclosure enhances the maximum electrical power P_{max}.

Using realistic values for the heat transfer coefficients h_{cold} and h_{hot}, the validity of the first approximation to equation (3), $\Delta T \ll T_{amb}$ can be assessed. The maximum temperature difference at simultaneous thermal and electrical impedance matching, according to equations (7) and (10), $\Delta T = \frac{\dot{Q}_{rad}(T_{amb})}{2K_{crad}}$. For $h_{cold} = 8\mathrm{Wm^{-2}K^{-1}}$, representing exposure to the ambient condition, ΔT is 3.42 K and 1.47 K for desert and tropics, respectively. For $h_{cold} = 0.05\ \mathrm{Wm^{-2}K^{-1}}$, representing the use of a vacuum enclosure, ΔT is 7.90 K and 3.40 K for desert and tropics, respectively. As noted from equation (7), the benefit of using a vacuum enclosure to amplify ΔT is offset by the heat conduction across the TEG unit. Therefore, the linear approximation is deemed valid $\Delta T < 0.03\ T_{amb}$, even when a vacuum enclosure is used, $\Delta T = 7.90$ K and $T_{amb} = 303.15$ K.

3.3. Maximum electrical power

Figure 5 shows the plot of maximum electrical power P_{max} generated by a single TEG unit, evaluated at the optimum radiative cooling surface area A_{opt}, according to equation (11), as a function of h_{cold}. With perfect thermal insulation of the radiative cooling surface ($h_{cold} = 0$), the maximum electrical power is around 10 mW in the desert and 2 mW in the tropics, enhanced by a factor, $\frac{(h_{rad}+h_{cold})^2}{h_{rad}^2}$. Where

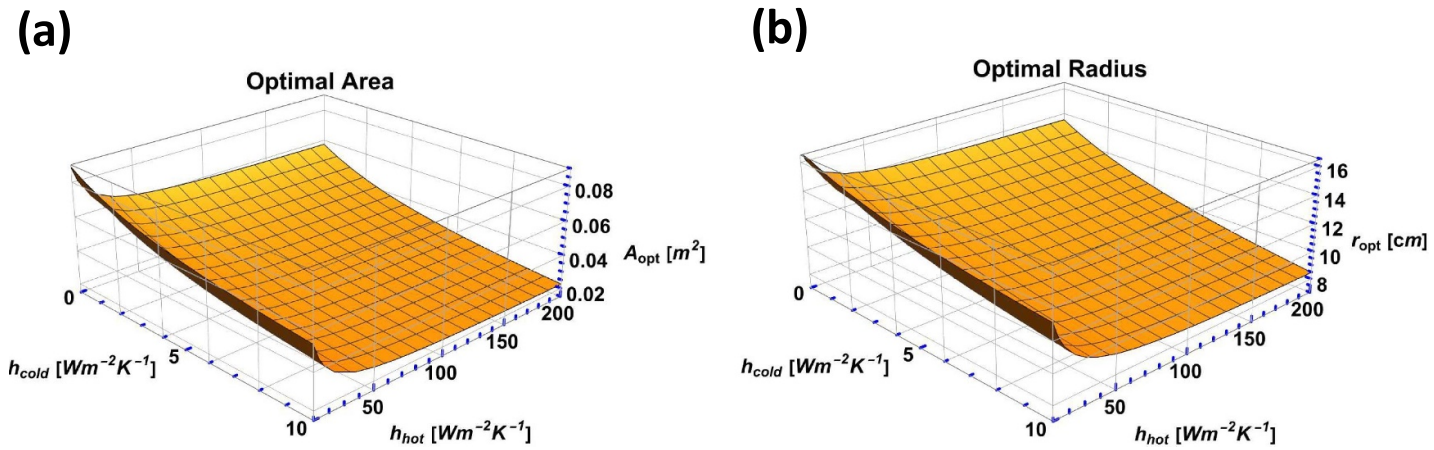

Figure 4. (a) Optimal area $A_{\rm opt}$ plotted as a function of $h_{\rm cold}$ and $h_{\rm hot}$. (b) The same plot as (a) but in terms of the optimal radius $r_{\rm opt}$ given by $A_{\rm opt} = \pi\, r_{\rm opt}^2$, assuming that the radiative cooling surface is of a circular shape.

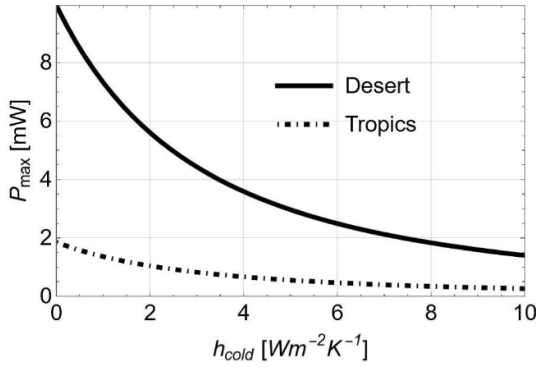

Figure 5. Plot of the maximum electrical power P_{max} for two climate conditions, desert and tropics.

$h_{cold} = 10\ \mathrm{Wm^{-2}K^{-1}}$, the enhancement factor for a perfect thermal insulation is 7.1. Since this enhancement factor is independent of other parameters, it remains the same across different climatic conditions. For example, with the radiative cooling surface is exposed to the ambient air ($h_{cold} = 10\ \mathrm{Wm^{-2}K^{-1}}$), the maximum electrical power is 1.40 mW in the desert, and 0.28 mW in the tropics. Recall from equation (11) that P_{max} does not depend on h_{hot}. This indicates that, for any heat transfer coefficient at the hot surface of the TEG, the electrical power can be optimised to the same maximum value by adjusting the area of the radiative cooling surface A_{opt}. For example, in the desert with a vacuum enclosure ($h_{cold} = 0.05\ \mathrm{Wm^{-2}K^{-1}}$), the optimal radius for $h_{hot} = 5\ \mathrm{Wm^{-2}K^{-1}}$ is 19.7 cm, while the optimal radius for $h_{hot} = 100\ \mathrm{Wm^{-2}K^{-1}}$ is 13.6 cm. Under these two conditions, the maximum achievable electrical power remains the same, 9.8 mW. This demonstrates that with a stronger heat sink at the hot surface, the total footprint of the device can be reduced.

The validity of the second approximation to equation (3), $P \ll \dot{Q}_{TEG}$, can be checked here. The total heat flowing across the TEG is given by $\dot{Q}_{TEG} = \mathrm{K}_{I=0}\sqrt{1+Z\bar{T}}\Delta T$, at the simultaneous thermal and electrical impedance matching condition. Assuming, with $h_{cold} = 8\mathrm{Wm^{-2}K^{-1}}$, the ratio or the efficiency $P_{max}/\dot{Q}_{TEG}$ is 0.00226 and 0.00097 for desert and tropics, respectively. With $h_{cold} = 0.05\ \mathrm{Wm^{-2}K^{-1}}$, representing the use of a vacuum enclosure, $P_{max}/\dot{Q}_{TEG}$ is 0.00302 and 0.00130 for desert and tropics, respectively. The second approximation is therefore deemed valid with the current exemplar system.

3.4. Maximum electrical power density

Often, the most limited resource for energy harvesting is the land coverage, and the power density $p_{max} = \frac{P_{max}}{A_{opt}}$ can be a critical parameter to optimise. Figures 6(a) and (b) show p_{max} as a function of h_{cold} and h_{hot}, respectively, in the desert and in the tropics. At each value of h_{cold} and h_{hot}, the optimal area A_{opt} is determined (figures 4(a) and 4(b)) and the maximum electrical power P_{max} is calculated (figure 5). The ratio of the two values yields the power density. The maximum power density p_{max} is achieved when h_{hot} is large and h_{cold} is small. This suggests that the intuitive design choice, to minimise the heat gain into the radiative cooling surface and to maximise the heat transfer coefficient from the hot surface to the ambient, indeed results in the optimisation of the electrical power density. When the heat transfer coefficient of the heat sink to the hot surface of the TEG is small, the power density approaches zero. However, as indicated by figure 5 and equation (11), the maximum electrical power does not depend on h_{hot}. Therefore, it can be concluded that a heat sink with a high heat transfer coefficient is essential for maximising the areal power density but not for maximising the electrical power of a given unit, since increasing the area of the radiative cooling surface can compensate for small h_{hot}. In the limit $h_{hot} \to \infty$, the power density is given by

$$p_{max,h_{hot}\to\infty} = \frac{Z(h_{rad}+h_{cold})}{4}\left(\frac{\dot{Q}_{rad}(T_{amb})}{K_{crad}}\right)^2 \frac{1}{\left(1+\sqrt{1+Z\bar{T}}\right)^2} \tag{16}$$

The maximum power density is therefore enhanced by a perfect thermal insulation by a factor $\frac{h_{rad}+h_{cold}}{h_{rad}}$. With $h_{cold} = 10\ \mathrm{Wm^{-2}K^{-1}}$, the power density enhancement is 2.7, not as large as the enhancement of the electrical power, where the enhancement factor is instead $\frac{(h_{rad}+h_{cold})^2}{h_{rad}^2}$. It is observed that the enhancement in areal power density achieved using a vacuum enclosure is not as pronounced as the enhancement in electrical power. This is because, as shown in figure 4 and discussed in the previous

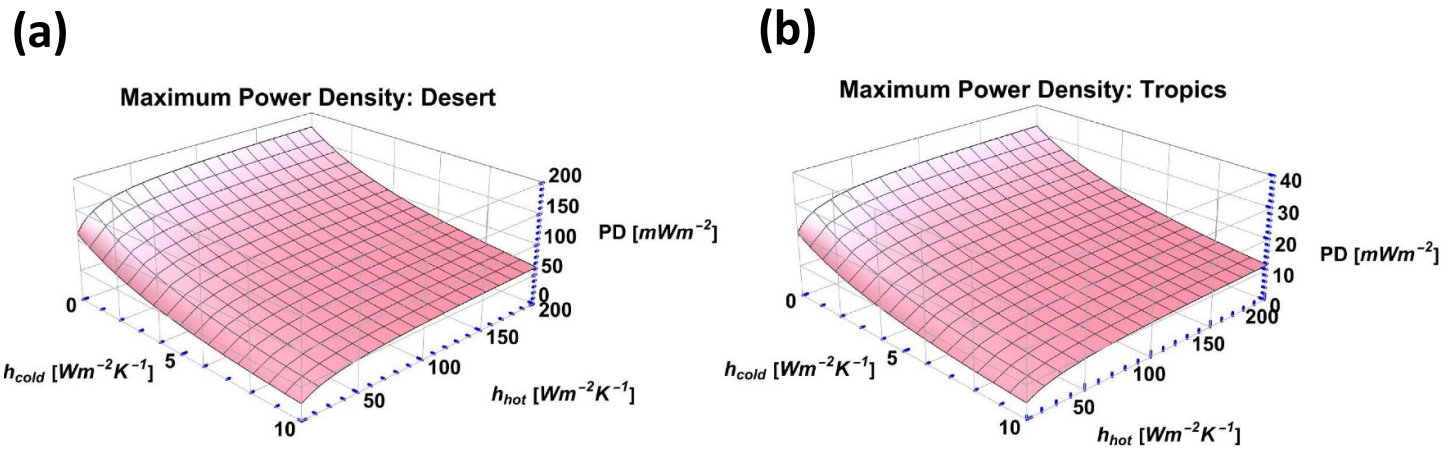

Figure 6. Plot of the power density in (a) desert and (b) tropics.

section, the optimal footprint area increases alongside the maximum electrical power and with greater thermal insulation of the radiative cooling surface. When considering the maximum power density as the primary parameter to optimise, the additional costs and complexity associated with a vacuum chamber should be carefully weighed against the gain in power density. For example, $h_{\text{cold}} = 0.05\ \text{Wm}^{-2}K^{-1}$ and $h_{\text{hot}} = 200\ \text{Wm}^{-2}K^{-1}$ - corresponding to a high-vacuum enclosure and a very large heat sink- the resulting areal power density of 172.4 mWm^{-2}, with an optimal radius of 13.4 cm in the desert. In contrast, a much simpler, therefore cheaper, configuration with the radiative cooling surface at ambient conditions, for example, $h_{\text{cold}} = 6\ \text{Wm}^{-2}K^{-1}$ and $h_{\text{hot}} = 20\ \text{Wm}^{-2}K^{-1}$, yields an areal power density of 56.0 mWm^{-2} with a smaller optimal radius of 11.9 cm. Although a detailed economic analysis will not be made here, a basic setup as depicted in figure 1 can be realised for less than $40 USD [13], whereas the cost of a vacuum system, especially the infrared-transmitting window, is considerably higher.

3.5. Workflow to identify optimal working conditions

Figure 7 presents a flowchart summarising the process used to identify the optimal working conditions. Three groups of system parameters are required. First, the radiative cooling and sky conditions are characterised by the average emissivity ε_{rcs} and the net radiative cooling power $\dot{Q}_{\text{rad}}(T_{\text{amb}})$. The average emissivity ε_{rcs} can be obtained from the measurement of $\varepsilon_{\text{rcs}}(\lambda,\theta)$ using an FT-IR spectrophotometer. The net radiative cooling power $\dot{Q}_{\text{rad}}(T_{\text{amb}})$ can be estimated from $\varepsilon_{\text{rcs}}(\lambda,\theta)$ and either measured or simulated downward atmospheric emission. $\dot{Q}_{\text{rad}}(T_{\text{amb}})$ can be directly measured without needing to determine downward atmospheric emission- for example, by attaching an electric heater to the radiative cooling surface facing the sky. The power dissipated at the electrical heater to maintain the surface at the ambient temperature corresponds to the net radiative cooling power $\dot{Q}_{\text{rad}}(T_{\text{amb}})$ under that specific sky condition. Second, the heat transfer coefficients at the two surfaces of the TEG must be determined. The radiative heat transfer coefficient h_{rad} directly follows from the average emissivity ε_{rcs}. h_{cold}, the heat transfer coefficient at the radiative cooling surface, can be estimated from the largest temperature drop ΔT_{c} achievable with the radiative cooling surface when it is not attached to the TEG, using the relation $h_{\text{cold}} \sim Q_{\text{rad}}(T_{\text{amb}})/\Delta T_{\text{c}}$. h_{hot}, the heat transfer coefficient at the hot side of the TEG, depends on the capacity of the heat sink attached to the hot surface. It can be measured by applying a known amount of heat to the heat sink over the contact area for the hot side of the TEG and recording the resulting temperature change of the heat sink. Third, the specifications of the TEG need to be known.

The contact thermal resistance K_{contact} can be obtained from the heat transfer coefficients. The simultaneous thermal and electrical impedance matching conditions, according to equation (10), can be obtained from the contact thermal resistance K_{contact} and the specifications of the TEG. The maximum electrical power P_{max} can be evaluated, according to equation (11), using all the system parameters. The optimal area A_{opt} of the radiative cooling surface follows from the thermal resistance balance condition of equation (10). The maximum power density can be obtained from $p_{\text{max}} = P_{\text{max}}/A_{\text{opt}}$.

3.6. Comparison of model with data

In the following, the maximum power density obtained from equation (16) will be compared with the reported values for the system depicted in figure 1, where a TEG is used to harvest electrical energy between the ambient surroundings and a radiative cooling surface facing the sky. In [39], Ioffe's formula (See S12 in section 1.2 of supplementary information) is numerically integrated to study the system's behaviour, considering a Marlow TG12–4, the same TEG as the exemplar system. Under the 'desert' condition specified above, $h_{\text{cold}} = 0.01\ \text{Wm}^{-2}K^{-1}$ and $h_{\text{hot}} = 20\ \text{Wm}^{-2}K^{-1}$ and a radiative cooling surface ($\varepsilon_{\text{rcs}} = 0.95$) with area $A = 0.0276\ \text{m}^2$ yields the areal power density around 110 mWm^{-2}. For the same parameters, equation (16) yields 110.44 mWm^{-2}, which largely agrees with the numerical results. Equations (15) and (16) predict that the areal power density can be maximised to 137.5 mWm^{-2}, with the optimised radiative cooling surface area $A = 0.0722\ \text{m}^2$.

The experimental results are less straightforward to compare, mainly because the sky conditions change with time and the exact value of the atmospheric emissivity ε_{atm} is often not measured or specified at the location of the measurement. However, for regions with extremely high or low humidity, the range of the atmospheric emissivity ε_{atm} is narrowed if a clear sky is assumed. For example, in [13], a radiative cooling surface ($\varepsilon_{\text{rcs}} = 0.95$) with a 10 cm radius is coupled to a TEG (Marlow TG12-4) at ambient conditions. With h_{cold} and h_{hot} estimated to be 7–9 $\text{Wm}^{-2}K^{-1}$, an areal power density of 25 mWm^{-2} was measured under a night sky in California. Assuming the 'desert' condition specified above, equation (16) gives, with $h_{\text{cold}} = h_{\text{hot}} = 8\ \text{Wm}^{-2}K^{-1}$, an areal power density of 24.5 mWm^{-2}, close to the reported measurement value. Equations (15) and (16) predict that the areal power density can be maximised to 27.9 mWm^{-2}, with the optimal radius of the radiative cooling surface at 14.4 cm.

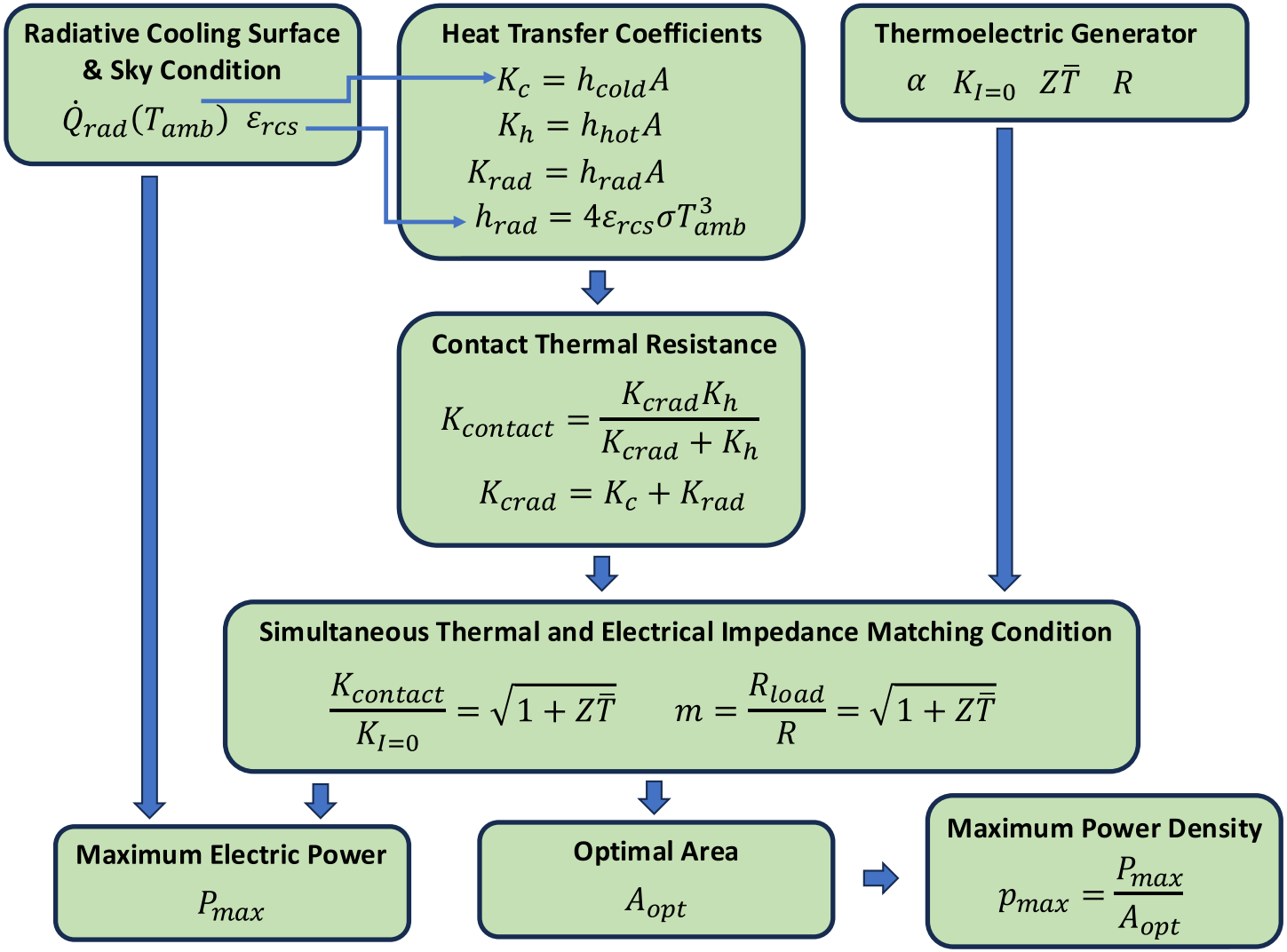

Figure 7. Flowchart summarising the process used to identify the optimal working conditions.

It is noted, however, that the choice of the radiative cooling surface area in this work was quite close to the optimum.

For another example, in [19], a radiative cooling surface ($\varepsilon_{rcs} = 0.60$) with a 4 cm radius was coupled to a Marlow TG12-4 TEG within a high vacuum chamber with a Germanium window with 85% transmissivity. Under a night sky in Singapore, an areal power density of 1.3 mWm^{-2} was measured. Assuming the 'tropics' condition specified above, $h_{hot} = 8\ Wm^{-2}K^{-1}$, and $h_{cold} = 0.05\ Wm^{-2}K^{-1}$ for the high-vacuum, equation (16) gives 2.1 mWm^{-2}. The discrepancy is attributed, apart from the inaccuracy of the assumed atmospheric emissivity, to the finite transmissivity of the window to the vacuum chamber, which reduces the radiative cooling power $\dot{Q}_{rad}(T_{amb})$. Equations (15) and (16) predict that the areal power density can be maximised to 14.0 mWm^{-2}, with the optimal radius of the radiative cooling surface at 20.2 cm. The radius of the radiative cooling surface in this work was chosen to be quite far from the optimum. However, given the restriction on the size of the infrared-transmitting window, it will be technically challenging to facilitate a radiative cooling surface with 40.4 cm diameter.

4. Conclusions and discussion

A fully analytical solution is presented for the thermoelectric generation with the ambient and the sky as the thermal resources. The main intuition is that the operating condition deviates substantially from the constant temperature condition as the radiative cooling power is typically insufficient to provide a constant temperature at the cold side, independently of the internal current and the thermal conduction from the hot side. This consequently leads to an increase in the internal electrical resistance and a decrease in the open circuit voltage of the TEG, the extent being dependent upon the degree of electrical and thermal impedance matching. Consequently, a simple analytical model, in which the hot side of the TEG is exactly at the ambient temperature and the thermal conductance across the TEG is assumed constant, does not explain certain system behaviours observed in either the experimental data or the black-box simulations.

To address this issue, derivations are made based on the thermal input and output power, without assuming any fixed temperature at either side of the TEG. This approach allows a rigorous description of the system, overcoming the limitations of over-simplified assumptions as follows. Firstly, the formalism treats the thermal conductance across the TEG as a function of the current and the temperature difference, fully accounting for the interplay between Fourier's law and Ohm's law. Secondly, to evaluate accurately the heat flux through the TEG, a finite heat transfer coefficient is assumed at the hot side. Consideration of the minute temperature difference between the hot side and the ambient is crucial for accurately estimating the electrical power and the efficiency.

As a result, analytical expressions are derived for the conditions to maximise the electrical power, as explicit functions of system parameters such as the radiative cooling surface area, the thermal isolation of the radiative cooling surface, and the heat transfer coefficient of the heat sink. Importantly, using the solutions, the optimal operating conditions can be identified without the need for iterative numerical calculations in which each parameter is varied incrementally.

The validity of the model rests upon the approximations based on two key assumptions, (1) $\Delta T \ll T_{amb}$ and (2) $P \ll \dot{Q}_{TEG}$. These approximations will not hold when the $Z\bar{T}$ value of a hypothetical TEG, in which $Z = \frac{\alpha^2}{RK_{I=0}}$, becomes sufficiently large. It should be noted that the validity of both approximations in the example system originates principally from the high degree of thermal conduction across the TEG, ΔT is less than several degrees even with a vacuum enclosure owing to the heat gain through the TEG and a large value of $Wm^{-2}K^{-1}$, proportional to $K_{I=0}$, maintains the overall efficiency at a low level. With the improved TEGs having a smaller $K_{I=0}$, the first approximation $\Delta T \ll (T_{amb})$should first be examined for validity. The presented model is, on the other hand, relatively robust to the increase of the Seebeck coefficient α. In an environment enabling a larger h_{cold} than the cooling power typically observed at the terrestrial level, for example at high altitude, the first assumption $\Delta T \ll (T_{amb})$ must also be examined for validity. When a selective emitter and a vacuum enclosure are used in a dry climate, the behaviour is largely linear up to $\Delta T \sim 30\ K$, approximately 10% of the ambient temperature, but beyond this value, the linear approximation underestimates ΔT [45]. This suggests that even in situations in which the validity of $\Delta T \ll (T_{amb})$ is unclear, the presented formalism will provide an estimate of the baseline performance.

Some of the parameters required to determine the optimal operating conditions are subject to dynamic changes in environmental conditions. The heat transfer coefficients, h_{cold} and h_{hot}, depend on wind speed, and the net radiative cooling power $\dot{Q}_{rad}(T_{amb})$ varies throughout the day and with the local weather conditions such as the cloud coverage, the sky emissivity and the solar irradiation. The model presented yields the steady-state solutions of the optimal conditions for fixed values of h_{cold}, h_{hot}

and $\dot{Q}_{\mathrm{rad}}(T_{\mathrm{amb}})$. This means that if the values of h_{cold}, h_{hot} and $\dot{Q}_{\mathrm{rad}}(T_{\mathrm{amb}})$ are given as a time series, the optimal conditions can be obtained also as a time series. However, the area of the radiative cooling surface, for example, is difficult to adjust *in situ* to such dynamic changes. In this case, the optimal design of the setup would have to be made considering the average values of the environmental parameters over a relevant period.

One of the principal findings of our model is the analytic derivation of the optimal area of the radiative cooling surface required to satisfy simultaneously the thermal and electrical impedance matching conditions. Increasing the area of the radiative cooling surface beyond this optimum reduces both the electrical power and the electrical power density. As an example, an off-the-shelf TEG with 127 p–n legs has been considered. The optimal radius of a near-blackbody radiative cooling surface ($\varepsilon_{\mathrm{rcs}} = 0.95$) exposed to ambient conditions ($h_{\mathrm{cold}} = h_{\mathrm{hot}} = 10\ \mathrm{Wm}^{-2}K^{-1}$) is 13.1 cm. In a dry climate, the maximum electrical power obtainable with the system is 1.4 mW, corresponding to an areal power density of 25.8 mWm^{-2}.

The analytical solutions also offer insights not necessarily obvious from numerical analyses. For example, the optimal area of the radiative cooling surface increases with improved thermal insulation. In contrast, the thermal insulation advantage offered by a vacuum enclosure is offset by the heat transfer from the hot surface through the TEG. Therefore, the additional costs and complexity of a vacuum chamber should be weighed carefully against the gain in power generation. In another example, the maximum electrical power is independent of the heat transfer coefficient of the hot side, whereas the maximum areal power density is not. The findings presented herein provide a detailed perspective on the relevant parameters and serve as a useful design guide, which would be critical for optimised performance if these systems were scaled up for large-area deployment.

The system analysed herein was considered for the purpose of renewable energy harvesting, but a related system could also be envisioned for a photodetection in the mid-infrared [58] or infrared target detection [59] of tuneable infrared emitters [60, 61].

Data availability statement

All data that support the findings of this study are included within the article (and any supplementary files).

Supplementary Information available at https://doi.org/10.1088/2515-7655/ae3642/data1.

Acknowledgment

This research is supported by the National Research Foundation, Singapore and A*STAR under its CQT Bridging Grant and by the National Research Foundation, Singapore through the National Quantum Office, hosted in A*STAR, under its Centre for Quantum Technologies Funding Initiative (S24Q2d0009). J. H. thanks Professor Christian Kurtsiefer for hosting him at the Centre for Quantum Technologies at NUS.

Conflict of interest

The authors have no conflicts to disclose.

Author contributions

Jaesuk Hwang 0009-0002-4387-8537
Conceptualization (equal), Formal analysis (equal), Validation (lead), Writing – original draft (lead), Writing – review & editing (equal)

Dario Narducci 0000-0002-3307-1070
Conceptualization (equal), Formal analysis (equal), Writing – review & editing (equal)

References

[1] Chaar L E and Zein N E 2011 Review of photovoltaic technologies *Renew. Sustain. Energy Rev.* **15** 2165–75
[2] Parida B, Iniyan S and Goic R 2011 A review of solar photovoltaic technologies *Renew. Sustain. Energy Rev.* **15** 1625–36
[3] Goetzberger A, Hebling C and Schock H-W 2003 Photovoltaic materials, history, status and outlook *Mater. Sci. Eng. R* **40** 1–46
[4] Polman A, Knight M, Garnett E C, Ehrler B and Sinke W C 2016 Photovoltaic materials: present efficiencies and future challenges *Science* **352** aad4424

[5] Thirugnanasambandam M, Iniyan S and Goic R 2010 A review of solar thermal technologies *Renew. Sustain. Energy Rev.* **14** 312–22
[6] Reddy V S, Kaushik S, Ranjan K and Tyagi S 2013 State-of-the-art of solar thermal power plants–a review *Renew. Sustain. Energy Rev.* **27** 258–73
[7] Zoui M A, Bentouba S, Stocholm J G and Bourouis M 2020 A review on thermoelectric generators: progress and applications *Energies* **13** 3606
[8] Baranowski L L, Snyder G J and Toberer E S 2012 Concentrated solar thermoelectric generators *Energy Environ. Sci.* **5** 9055–67
[9] Shoeibi S, Kargarsharifabad H, Sadi M, Arabkoohsar A and Mirjalily S A A 2022 A review on using thermoelectric cooling, heating, and electricity generators in solar energy applications *Sustain. Energy Technol. Assess.* **52** 102105
[10] Sundarraj P, Maity D, Roy S S and Taylor R A 2014 Recent advances in thermoelectric materials and solar thermoelectric generators–a critical review *RSC Adv.* **4** 46860–74
[11] Hossain M M and Gu M 2016 Radiative cooling: principles, progress, and potentials *Adv. Sci.* **3** 1500360
[12] Fan S and Li W 2022 Photonics and thermodynamics concepts in radiative cooling *Nat. Photon.* **16** 182–90
[13] Raman A P, Li W and Fan S 2019 Generating light from darkness *Joule* **3** 2679–86
[14] Zhao B, Hu M, Ao X, Xuan Q, Song Z and Pei G 2021 Is it possible for a photovoltaic-thermoelectric device to generate electricity at night? *Sol. Energy Mater. Sol. Cells* **228** 111136
[15] Omair Z, Assawaworrarit S, Fan L, Jin W and Fan S 2022 Radiative-cooling-based nighttime electricity generation with power density exceeding 100 mW/m2 *iScience* **25** 104858
[16] Khan S, Cheema T A, Abbas A, Ullah R and Park C W 2023 Impact of environmental factors on night-time electricity generation using thermoelectric generator *Sustain. Energy Technol. Assess.* **56** 103000
[17] Assawaworrarit S, Omair Z and Fan S 2022 Nighttime electric power generation at a density of 50 mW/m2 via radiative cooling of a photovoltaic cell *Appl. Phys. Lett.* **120** 143901
[18] Lv S, Li Z, Zhang B, Ren J, Ji Y and Yang J 2023 Study on coupling characteristics and parameter optimization of thermoelectric generation via radiative cooling (RC-TE) system *Appl. Therm. Eng.* **228** 120444
[19] Hwang J 2025 Harvesting solar energy without excess environmental heating *Cell Rep. Phys. Sci.* **6** 102345
[20] Assawaworrarit S, Zhou M, Fan L and Fan S 2025 Nighttime electric power generation at a density of 350 mW/m2 via radiative cooling *Cell Rep. Phys. Sci.* **6** 102362
[21] Fan L, Li W, Jin W, Orenstein M and Fan S 2020 Maximal nighttime electrical power generation via optimal radiative cooling *Opt. Express* **28** 25460–70
[22] Nøland J K, Auxepaules J, Rousset A, Perney B and Falletti G 2022 Spatial energy density of large-scale electricity generation from power sources worldwide *Sci. Rep.* **12** 21280
[23] Alajlan A M, Dang S and Gan Q 2024 Enhanced nighttime power generation and photovoltaic cooling in photovoltaic-thermoelectric hybrid systems *Energy Convers. Manage.: X* **22** 100580
[24] Zaite A, Belouaggadia N, Abid C, Kaiss A and Imghoure O 2024 Performance enhancement of a photovoltaic-thermal thermoelectric collector using night radiative cooling *Appl. Energy* **364** 123108
[25] Kumar R, Montero F J, Lamba R, Vashishtha M and Upadhyaya S 2023 Thermal management of photovoltaic-thermoelectric generator hybrid system using radiative cooling and heat pipe *Appl. Therm. Eng.* **227** 120420
[26] Yang J, Han J, Duan L, Zhu W, Liang W and Mou C 2024 Investigation on a novel hybrid system based on radiative sky cooling and split thermoelectric cooler driven by photovoltaic cell *Renew. Energy* **229** 120798
[27] Lv S, Ji Y, Qian Z, He W, Hu Z and Liu M 2021 A novel strategy of enhancing sky radiative cooling by solar photovoltaic-thermoelectric cooler *Energy* **219** 119625
[28] Guo J and Huai X 2023 Maximizing electric power through spectral-splitting photovoltaic-thermoelectric hybrid system integrated with radiative cooling *Adv. Sci.* **10** 2206575
[29] Ishii S, Miura A, Nagao T and Uchida K-I 2021 Simultaneous harvesting of radiative cooling and solar heating for transverse thermoelectric generation *Sci. Technol. Adv. Mater.* **22** 441–8
[30] Zhang W-W, Guo Y-M, He M-J, Ren Y-T, Gao B-H and Qi H 2024 Self-adaptive photothermal/radiative cooling-thermoelectric conversion system for 24 h electricity generation *Appl. Therm. Eng.* **243** 122603
[31] Wang C-H, Chen H, Jiang Z-Y and Zhang X-X 2023 Design and experimental validation of an all-day passive thermoelectric system via radiative cooling and greenhouse effects *Energy* **263** 125735
[32] Zhang S, Wu Z, Liu Z and Hu Z 2023 An emerging energy technology: self-uninterrupted electricity power harvesting from the sun and cold space *Adv. Energy Mater.* **13** 2300260
[33] Jeong I H, Park S W, Kim M S, Kim J T and Lee G J 2023 Parabolic mirror-assisted thermoelectric and radiative cooling system for maximizing power generation utilizing solar and outer space thermodynamic resources *Adv. Mater. Interfaces* **10** 2300573
[34] Liu Y, Xie Y, Chen H, Liao J, Lu Y, Lan D and Wang C 2024 Design and experimental study of a compact thermoelectric device driven by solar heating and radiative cooling *Next Energy* **4** 100146
[35] Hou M, Chen H, Li S, Zhang X, Chen J, Jiang Z, Wang C, Lai N C, Ding Y and Tri-Mode Photothermal A 2025 Phase-change, and radiative-cooling film for all-day thermoelectric generation *Adv. Mater.* **37** 2505601
[36] Apertet Y, Ouerdane H, Glavatskaya O, Goupil C and Lecoeur P 2012 Optimal working conditions for thermoelectric generators with realistic thermal coupling *Europhys. Lett.* **97** 28001
[37] Zhu Y, Newbrook D W, De Groot C and Huang R 2023 Comprehensive analysis of radiative cooling enabled thermoelectric energy harvesting *J. Phys.* **5** 025002
[38] Ji Y and Lv S 2023 Comprehensive research on a simple and efficient radiative cooling driving thermoelectric generator system for nighttime passive power generation *Appl. Therm. Eng.* **219** 119560
[39] Zhao B, Pei G and Raman A P 2020 Modeling and optimization of radiative cooling based thermoelectric generators *Appl. Phys. Lett.* **117** 163903
[40] Smith G B 2009 Amplified radiative cooling via optimised combinations of aperture geometry and spectral emittance profiles of surfaces and the atmosphere *Sol. Energy Mater. Sol. Cells* **93** 1696–701
[41] Martin M and Berdahl P 1984 Characteristics of infrared sky radiation in the United States *Sol. Energy* **33** 321–36
[42] Berk A, Conforti P, Kennett R, Perkins T, Hawes F and van den Bosch J 2014 MODTRAN (R) 6: a major upgrade of the MODTRAN (R) radiative transfer code *20th SPIE Conf. on Algorithms and Technologies for Multispectral, Hyperspectral, and Ultraspectral Imagery* (*Baltimore, MD*)s
[43] Martin M and Berdahl P 1984 Summary of results from the spectral and angular sky radiation measurement program *Sol. Energy* **33** 241–52

[44] Hwang J 2024 Daytime radiative cooling under extreme weather conditions *Adv. Energy Sustain. Res.* **5** 2300239
[45] Hwang J 2024 Climate-dependent enhancement of radiative cooling with mirror structures *J. Photon. Energy* **14** 028001
[46] Wong R Y, Tso C, Jeong S, Fu S and Chao C Y 2023 Critical sky temperatures for passive radiative cooling *Renew. Energy* **211** 214–26
[47] Yu X X, Chan J Q and Chen C 2021 Review of radiative cooling materials: performance evaluation and design approaches *Nano Energy* **88** 106259
[48] Raman A P, Anoma M A, Zhu L X, Rephaeli E and Fan S H 2014 Passive radiative cooling below ambient air temperature under direct sunlight *Nature* **515** 540
[49] Gentle A R and Smith G B 2015 A subambient open roof surface under the mid-summer sun *Adv. Sci.* **2** 1500119
[50] Gomez M, Reid R, Ohara B and Lee H 2013 Influence of electrical current variance and thermal resistances on optimum working conditions and geometry for thermoelectric energy harvesting *J. Appl. Phys.* **113** 174908
[51] Berdahl P 2021 Retrospective on the resource for radiative cooling *J. Photon. Energy* **11** 042106
[52] Berdahl P and Fromberg R 1982 The thermal radiance of clear skies *Sol. Energy* **29** 299–314
[53] Castro P and Happ W 1960 Performance of a thermoelectric converter under constant heat flux operation *J. Appl. Phys.* **31** 1314–7
[54] Narducci D 2011 Do we really need high thermoelectric figures of merit? A critical appraisal to the power conversion efficiency of thermoelectric materials *Appl. Phys. Lett.* **99** 102104
[55] Chen Z, Zhu L, Li W and Fan S 2019 Simultaneously and synergistically harvest energy from the sun and outer space *Joule* **3** 101–10
[56] Chen Z, Zhu L X, Raman A and Fan S H 2016 Radiative cooling to deep sub-freezing temperatures through a 24-h day-night cycle *Nat. Commun.* **7** 13729
[57] Ao X, Li B, Zhao B, Hu M, Ren H, Yang H, Liu J, Cao J, Feng J and Yang Y 2022 Self-adaptive integration of photothermal and radiative cooling for continuous energy harvesting from the sun and outer space *Proc. Natl Acad. Sci.* **119** e2120557119
[58] Chen Y, Wang Y, Wang Z, Gu Y, Ye Y, Chai X, Ye J, Chen Y, Xie R and Zhou Y 2021 Unipolar barrier photodetectors based on van der Waals heterostructures *Nat. Electron.* **4** 357–63
[59] Hu W, Ye Z, Liao L, Chen H, Chen L, Ding R, He L, Chen X and Lu W 2014 128× 128 long-wavelength/mid-wavelength two-color HgCdTe infrared focal plane array detector with ultralow spectral cross talk *Opt. Lett.* **39** 5184–7
[60] Kang Q, Guo K and Guo Z 2023 A tunable infrared emitter based on phase-changing material GST for visible-infrared compatible camouflage with thermal management *Phys. Chem. Chem. Phys.* **25** 27668–76
[61] Kang Q, Li D, Wang W, Guo K and Guo Z 2021 Multiband tunable thermal camouflage compatible with laser camouflage based on GST plasmonic metamaterial *J. Appl. Phys.* **55** 065103